J Sign Process Syst (2018) 90:1495–1505
https://doi.org/10.1007/s11265-017-1303-1

Low-complexity, Multi Sub-band Digital Predistortion

Novel Algorithms and SDR Verification

Chance Tarver[1] · Mahmoud Abdelaziz[2] · Lauri Anttila[2] · Mikko Valkama[2] · Joseph R. Cavallaro[1]

Received: 19 June 2017 / Revised: 6 September 2017 / Accepted: 18 October 2017 / Published online: 15 November 2017

Abstract The nonlinearities of power amplifiers combined with non-contiguous transmissions found in modern, frequency-agile, wireless standards create undesirable spurious emissions through the nearby spectrum of data carriers. Digital predistortion (DPD) is an effective way of combating spurious emission violations without the need for a significant power reduction in the transmitter leading to better power efficiency and network coverage. In this paper, an iterative, multi sub-band version of the sub-band DPD, proposed earlier by the authors, is presented. The DPD learning is iterated over intermodulation distortion (IMD) sub-bands until a satisfactory performance is achieved for each of them. A sequential DPD learning procedure is also presented to reduce the hardware complexity when higher order nonlinearities are incorporated in the DPD learning. Improvements in the convergence speed of the adaptive DPD learning are also achieved via incorporating a variable learning rate and interpolation of previously trained DPD coefficients. A WARPLab implementation of the proposed DPD is also shown with excellent suppression of the targeted spurious emissions.

Keywords Adaptive filters · Carrier aggregation · Digital predistortion · Nonlinear distortion · Power amplifier · Software-defined radio · Spectrally-agile radio · Spurious emission

✉ Chance Tarver
cat12@rice.edu

Joseph R. Cavallaro
cavallar@rice.edu

[1] Department of Electrical and Computer Engineering, Rice University, Houston, TX 77005, USA

[2] Department of Electronics and Communication Engineering, Tampere University of Technology, Tampere, Finland

1 Introduction

Mobile devices need to access more radio spectrum to meet the increasing data-rate demands of mobile users. This is particularly challenging when we compound this with the growing number of active wireless devices in the world today [1]. This leads to what is referred to as spectrum scarcity and fragmentation [2, 3]. In scenarios where there is little available bandwidth, it may be necessary to aggregate spectrum opportunistically, potentially across multiple bands non-contiguously. This sort of frequency-agile system has been adopted in protocols and standards such as in LTE-Advanced with carrier aggregation [4] and will likely also play a role in 5G communications [5].

For cases where spectrum is aggregated in a non-continuous manner, challenges arise in the radio frontend design. In particular, the power amplifier (PA) becomes problematic. The PA is inherently a nonlinear device [6], and whenever non-contiguous signals pass through this nonlinearity, they intermodulate creating intermodulation distortion (IMD) components throughout the nearby spectrum as illustrated in Fig. 1. For example, if carriers exist at radio frequencies f_1 and f_2, there will be third-order IMD products (IM3s) at frequencies of $2f_1 - f_2$ and $2f_2 - f_1$. These spurious emissions or "spurs" could interfere with other users or with a device's own receiver in a frequency-division duplexing scenario [7]. If severe enough, they may violate emission requirements in standards such as the 3GPP LTE-Advanced or other FCC standards [8–11].

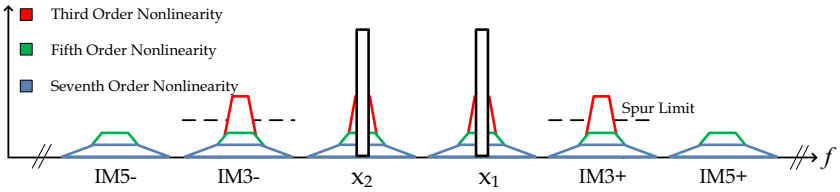

Figure 1 Power spectral density of a non-contiguous signal after being applied through a nonlinear PA. Intermodulation of the main carriers, x_1 and x_2, cause distortion throughout the nearby spectrum. For example, the third-order intermodulation distortion products (IMDs) are shown as IM3- and IM3+. Each IMD is the sum of multiple nonlinearity components. Here we show the contribution of each nonlinear order up to the seventh in each of the IMD products.

The undesirable effects of the PA nonlinearities are exacerbated by modern, multicarrier signals such as OFDM due to their high peak-to-average power ratio (PAPR) [6]. Techniques such as crest factor reduction (CFR) can help reduce the PAPR of these signals by many dB by limiting the peak power through clipping and filtering. However, CFR doesn't correct for the nonlinearities of the PA and may come at the cost of a poorer error-vector magnitude [12].

In conjunction with CFR, to avoid violating the strict emission requirements, devices may need to also considerably back off their transmit power from the nominal maximum value (e.g., +23 dBm in 3GPP LTE uplink) so that the PA operates in a more linear region. However, reducing the transmit power in order to satisfy the emission mask will necessarily reduce the uplink coverage and the energy efficiency of the PA. [8, 13–17].

An alternative to power back-off is digital predistortion (DPD). DPD is a signal processing technique that requires sampling the output of the PA to learn its nonlinearities and then applying an inverse of them in the digital baseband signal to cancel the effect of the PA's nonlinearities. This can have the effect of dramatically reducing spurious emissions and other nonlinear effects [17].

However, to cancel a nonlinearity, we have to also be able to observe it. For many carrier aggregation scenarios, the carriers may be spaced hundreds of MHz apart. This would lead to their IMD products being spaced even farther apart so that the observation bandwidth necessary to mitigate the spurious emissions becomes infeasible for many analog-to-digital converters (ADCs) and radio-frequency (RF) downconverters [18].

This issue is quickly becoming more prevalent in that carrier aggregation is now almost commonplace. Since its 2011 debut in LTE Release 10, it has made its way from the standards down to commercial implementations. Many networks already provide support for up to three carriers on the downlink [19], and many consumer devices also support it with system-on-chips such as the Snapdragon 835 supporting four downlink carriers and two uplink carriers [20]. However, most DPD solutions do not completely consider the carrier aggregation scenario. For example, in [18], the effects of intermodulation are considered, but only the bandwidth around the main carrier is linearized.

To combat this, the authors introduced a sub-band DPD method in [16]. However, the IM3 sub-bands were considered separately while not taking into consideration the mutual effect of each of the IM3 sub-band DPDs over the other. An FPGA implementation of this solution has also been presented by the authors in [21] demonstrating real-time processing of the adaptive DPD learning solution.

An extension of the DPD solution in [16, 21] was proposed in [22], where an iterative learning algorithm is used between the right and left IM3 sub-bands until they are both properly suppressed. A WARPLab implementation of an iterative version of this higher order sub-band DPD was also presented with additional ideas added to reduce the complexity and/or improve the learning speed of the proposed DPD. Moreover, in [23], higher nonlinearity orders were introduced in addition to the third-order nonlinearity processing in [16, 21].

In this paper, we extend the work from [22] to include processing for the fifth-order IMD products (IM5) and include new interpolation based speed-up methods. In summary, this paper includes:

- An iterative version of the previously proposed sub-band DPD. This solution iterates between the different spurious components, such as the IM3+, IM3-, IM5+, and IM5- until a satisfactory performance is achieved for each of them. This improves the flexibility and potentially reduces complexity when compared to a full-band DPD system in that learning can be focused only on sub-bands that are in violation of emission limits and only a single RF feedback path is necessary. This comes at a cost of additional latency when compared to full-band DPD.
- The learning of the higher-order nonlinearities in each sub-band is done sequentially, one basis function at a time in ascending order. This has the advantage of reducing the hardware complexity by essentially using one learning module for all the nonlinearity orders. An additional flexibility advantage is that we can stop

adding higher orders in the learning phase once a sufficient spurious emission suppression is achieved, thus further reducing the complexity. However, this comes at a cost of additional latency.

– To improve the convergence speed of the proposed solution, two modifications have been adopted in this paper. The first is using a variable learning rate during the DPD coefficient learning to have a fast convergence during the initial phase of the learning while not sacrificing the steady-state error. The second modification is that the DPD coefficients are stored once they are converged. When transmitting, the previous acts as a starting point for learning anytime the same carrier configuration is transmitted again. For transmissions with new configurations, we can interpolate from stored values to help start training from a value close to the final value.
– A WARPLab implementation is done demonstrating effective performance of the proposed solution using real hardware equipment.

This paper is organized as follows. In Section II, the modeling of the spurious emissions at the IM3 sub-bands and their mutual effects are presented. The proposed iterative sub-band DPD processing is also introduced in this section. In Section III, sequential learning of the DPD coefficients is proposed to reduce the hardware complexity. In Section IV, two methods are proposed for improving the convergence time. In Section V, the overall DPD system flow is presented. In Section VI, we show the results from testing the proposed algorithms on the WARPLab platform. Finally, in Section VII, we conclude the paper.

2 Spurious Component Modeling and Iterative IM3 Sub-band DPD Processing

In [16], a decorrelation-based sub-band DPD was proposed to mitigate the spurious emissions at the IM3± sub-bands. However, the mutual effect of, for example, the IM3+ sub-band DPD on the other sub-bands was not taken into consideration. In this work, we propose an iterative sub-band DPD that starts with linearizing the most extreme sub-band, and then after applying the sub-band DPD, the learning is switched to another sub-band. Since each of the IM3± and IM5± sub-band DPDs has an effect on the other sub-bands, the proposed DPD iterates the learning between each of the considered sub-bands until the spurious emissions are sufficiently suppressed.

To further illustrate this behavior, a mathematical analysis is introduced in this section to show the impact of the IM3+ sub-band DPD on the IM3- sub-band when a dual carrier signal is applied to a nonlinear PA. This analysis will provide a theoretical foundation and motivation for our work. For simplicity of the presentation, we restrict our analysis in this section to third-order nonlinearity. However, in the actual WARPLab experiments, higher order nonlinearities are included in the DPD processing. The analysis is carried out at composite baseband equivalent level, and the two component carriers (CC's) are assumed to be separated by $2f_{If}$. Thus, the composite baseband equivalent PA input and output signals, $x(n)$ and $y(n)$, read

$$x(n) = x_1(n)e^{j2\pi\frac{f_{If}}{f_s}n} + x_2(n)e^{-j2\pi\frac{f_{If}}{f_s}n}, \quad (1)$$

$$y(n) = \beta_1 x(n) + \beta_3|x(n)|^2 x(n), \quad (2)$$

where β_1 and β_3 are unknown PA coefficients, and $x_1(n)$ and $x_2(n)$ are the baseband equivalents of the input CCs. Through direct substitution of Eq. 1 in Eq. 2, the baseband equivalent positive and negative IM3 terms read

$$y_{IM3_+}(n) = \beta_3 x_2^*(n)x_1^2(n), \quad (3)$$

$$y_{IM3_-}(n) = \beta_3 x_1^*(n)x_2^2(n). \quad (4)$$

The idea proposed in [16], for suppressing the IMD at the IM3+ sub-band for example, is to inject a proper additional low-power cancelation signal to Eq. 1, located at three times f_{If}, such that spurious emission at the IM3+ sub-band at the PA output is suppressed. Stemming from the signal structure in Eq. 3, the injection signal is of the form $x_2^*(n)x_1^2(n)$ but should be scaled properly with a complex DPD coefficient denoted here by α. Thus, incorporating such DPD processing, the composite baseband equivalent PA input signal now reads

$$\tilde{x}(n) = x_1(n)e^{j2\pi\frac{f_{If}}{f_s}n} + x_2(n)e^{-j2\pi\frac{f_{If}}{f_s}n} + \alpha(x_2^*(n)x_1^2(n))e^{j2\pi\frac{3f_{If}}{f_s}n}. \quad (5)$$

Substituting now $\tilde{x}(n)$ in Eq. 2, the IM3 components at PA output read

$$\tilde{y}_{IM3_+}(n) = (\beta_3 + \beta_1\alpha)x_2^*(n)x_1^2(n) + 2\beta_3\alpha(|x_1(n)|^2 + |x_2(n)|^2)x_2^*(n)x_1^2(n) + \beta_3|\alpha|^2\alpha|x_1(n)|^4|x_2(n)|^2x_2^*(n)x_1^2(n), \quad (6)$$

$$\tilde{y}_{IM3_-}(n) = \beta_3 x_1^*(n)x_2^2(n) + \boxed{2\beta_3\alpha^*|x_1(n)|^2x_1^*(n)x_2^2(n)}. \quad (7)$$

It can be seen from Eqs. 6 and 7 that the spurious emissions at both IM3 sub-bands are dependent on the DPD parameter α, despite the cancelation signal being injected only at the IM3+ sub-band. In particular, an additional fifth-order term which depends on α appears at the IM3- sub-band, which is shown inside the box in Eq. 7. Despite the magnitude of this term being quite small, it becomes considerable when the PA exhibits strong nonlinearities. This represents the theoretical basis of the mutual effect the IM3+ sub-band DPD has on the two IM3 sub-bands.

In [16], the learning of the DPD parameter α, for the IM3+ sub-band, for example, was formulated to minimize

the correlation between the IMD at the considered IM3 sub-band and the distortion basis $x_2^*(n)x_1^2(n)$. This correlation minimization will eventually minimize the distortion at the considered sub-band effectively, as demonstrated in [16, 21]. However, optimizing the DPD parameter α to minimize the power at the IM3+ sub-band, will affect the IM3- sub-band as well, as shown in Eqs. 6 and 7.

That is why an iterative sub-band DPD learning is proposed in this paper in the case that multiple IMD sub-bands are required to be mitigated effectively. First, we start by learning the DPD coefficients for the most extreme IMD sub-band, then after injecting its DPD cancelation signal, the emissions at other sub-bands are raised a little above their original levels due to the mutual effect described earlier. In the case that the IM3+ is the most extreme, learning begins there. Then, the DPD learning may switch to the IM3- sub-band, which then also affects the IM3+ sub-band. An extra iteration may be required at previously learned sub-bands so that the spurious emissions are all reduced to appropriate levels. This will be demonstrated in the WARPLab experimental results in Section 6. This method also has a practical, hardware benefit in that only a single RF feedback path is necessary. The downconverter in the feedback path will simply be re-tuned to each of the sub-bands during training.

In the following sections, modifications are introduced to the proposed sub-band DPD in order to reduce the complexity, improve the convergence speed, or both. These aspects are particularly important for mobile devices, which is the main scope of this work.

3 Sequential Learning of IM3 Sub-Band DPD Coefficients

A detailed analysis of the nonlinear distortions at the IM3 and IM5 sub-band has been done in [23] when a ninth-order PA is excited with a dual carrier signal as in Eq. 1. We hereby present the distortion components up to the ninth order at the IM3+ sub-band, which read

$$u_3^{3+}(n) = x_2^*(n)x_1^2(n), \tag{8}$$

$$u_5^{3+}(n) = u_3^+(n) \times (2|x_1(n)|^2 + 3|x_2(n)|^2), \tag{9}$$

$$u_7^{3+}(n) = u_3^+(n) \times (3|x_1(n)|^4 + 6|x_2(n)|^4 + 12|x_1(n)|^2|x_2(n)|^2), \tag{10}$$

$$u_9^{3+}(n) = u_3^+(n) \times (4|x_1(n)|^6 + 10|x_2(n)|^6 + 30|x_1(n)|^4|x_2(n)|^2 + 40|x_1(n)|^2|x_2(n)|^4). \tag{11}$$

Similarly, for the IM3- sub-band, the distortions terms $u^{3-}(n)$ are simply obtained by interchanging $x_1(n)$ and $x_2(n)$ in Eqs. 8–11. The distortion components up to the ninth order at the IM5+ sub-band read

$$u_5^{5+}(n) = (x_2^*(n))^2x_1^3(n), \tag{12}$$

$$u_7^{5+}(n) = u_5^{5+}(n) \times (4|x_1(n)|^2 + 3|x_2(n)|^2), \tag{13}$$

$$u_9^{5+}(n) = u_7^{5+}(n) \times (10|x_1(n)|^4 + 6|x_2(n)|^4 + 20|x_1(n)|^2|x_2(n)|^2). \tag{14}$$

Similarly, for the IM5- sub-band, the distortions terms $u^{5-}(n)$ are simply obtained by interchanging $x_1(n)$ and $x_2(n)$.

The proposed DPD was based on injecting the above basis functions at the IM3+ sub-band with proper scaling such that the distortion at the IM3+ sub-band is minimized. The composite baseband equivalent PA input signal with Q^{th} order sub-band DPD processing thus reads

$$\tilde{x}(n) = x(n) + \left[\sum_{\substack{q=3 \\ q \text{ odd}}}^{Q} \alpha_{q,n}^+ \star u_q^+(n)\right] e^{j2\pi \frac{3f_{If}}{f_s}n} \tag{15}$$

The q^{th} order DPD coefficients $\alpha_{q,n}^+$ are obtained such that the correlation is minimized between the nonlinear distortion observed at the PA output at the IM3+ sub-band, and the nonlinear basis functions in Eqs. 8–11. This is formulated as a simple block-adaptive learning approach, where the following vector based notations are defined

$$\boldsymbol{\alpha}_q^+(m) = [\alpha_{q,0}^+(m)\ \alpha_{q,1}^+(m)\ \ldots\ \alpha_{q,N}^+(m)]^T, \tag{16}$$

$$\bar{\boldsymbol{\alpha}}^+(m) = [\boldsymbol{\alpha}_3^+(m)^T\ \boldsymbol{\alpha}_5^+(m)^T\ \ldots\ \boldsymbol{\alpha}_Q^+(m)^T]^T, \tag{17}$$

$$\mathbf{u}_q^+(n_m) = [u_q^+(n_m)\ u_q^+(n_m-1)\ \ldots\ u_q^+(n_m-N)]^T, \tag{18}$$

$$\bar{\mathbf{u}}^+(n_m) = [\mathbf{u}_3^+(n_m)^T\ \mathbf{u}_5^+(n_m)^T\ \ldots\ \mathbf{u}_Q^+(n_m)^T]^T, \tag{19}$$

$$\bar{\mathbf{U}}^+(m) = [\bar{\mathbf{u}}^+(n_m)\ \ldots\ \bar{\mathbf{u}}^+(n_m+M-1)], \tag{20}$$

where N denotes the DPD filter memory depth, and n_m denotes the first sample of block m, with block size M. Consequently, the DPD block-adaptive parameter learning update then reads

$$\mathbf{e}^+(m) = [\tilde{y}_{IM3_+}(n_m)\ \ldots\ \tilde{y}_{IM3_+}(n_m+M-1)]^T, \tag{21}$$

$$\bar{\boldsymbol{\alpha}}^+(m+1) = \bar{\boldsymbol{\alpha}}^+(m) - \mu\, \bar{\mathbf{U}}^+(m)\mathbf{e}^{+*}(m), \tag{22}$$

where $\tilde{y}_{IM3_+}(n)$ denotes the baseband equivalent observation of the PA output at the IM3+ sub-band with the current DPD coefficients, and $\mathbf{e}^{+*}(m)$ refers to the element-wise conjugated error signal vector, while $\bar{\mathbf{U}}^+(m)$ denotes the filter input data matrix, all within the processing block m. The obtained new DPD coefficients $\bar{\boldsymbol{\alpha}}^+(m+1)$ are then applied to the next block of samples, as illustrated in [21].

In order to reduce the hardware complexity of the DPD, a sequential learning of the DPD coefficients is adopted in this paper instead of learning the DPD coefficients for all the nonlinearity orders concurrently. The idea is to first train the DPD for the third-order coefficient, and after injecting

the scaled third-order basis function at the target IM3 sub-band, we start training for the fifth-order coefficient using the residual IMD at the target sub-band, and so on. This proposed learning algorithm has two advantages. The first is that only one hardware module needs to be used for training all the DPD nonlinearity orders thus reducing the hardware overhead due to DPD learning, which is an important aspect, especially for small devices. The second advantage is that we can stop training the DPD once a sufficient performance is achieved. For example, if after doing the third-order training, the transmitter already satisfies the emission limits, then there is no need to train the DPD for higher orders. This will save the complexity in both the DPD training phase and in the actual DPD filtering as well.

However, for fast and smooth learning of the proposed sub-band DPD coefficients, a basis function orthogonalization procedure was proposed earlier in [23]. In this paper, we use an orthogonalization procedure which allows us to learn the DPD coefficients with different orders sequentially instead of concurrently. The idea of the orthogonalization and learning procedure in this paper is to generate the third-order basis function and train the DPD for this basis function. Then the projection of the third-order basis function onto the fifth-order basis function is subtracted from the fifth-order basis function in order to obtain the new orthogonalized fifth-order basis function, which is then used to train the DPD for the fifth-order nonlinearity, and so on. Once the spurious emissions satisfy the emission regulations, the DPD training is stopped to save further higher-order processing that may not be required, depending on the transmission scenario and TX power level. Using the standard vector dot product, the new orthogonalized basis functions $v_q^{\pm}(n)$ used for DPD learning thus read

$$v_3^{\pm}(n) = u_3^{\pm}(n), \tag{23}$$

$$v_5^{\pm}(n) = u_5^{\pm}(n) - \frac{dot(u_5^{\pm}(n), v_3^{\pm}(n))}{||v_3^{\pm}(n)||^2} v_3^{\pm}(n), \tag{24}$$

$$\begin{aligned} v_7^{\pm}(n) = {} & u_7^{\pm}(n) - \frac{dot(u_7^{\pm}(n), v_3^{\pm}(n))}{||v_3^{\pm}(n)||^2} v_3^{\pm}(n) \\ & - \frac{dot(u_7^{\pm}(n), v_5^{\pm}(n))}{||v_5^{\pm}(n)||^2} v_5^{\pm}(n), \end{aligned} \tag{25}$$

$$\begin{aligned} v_9^{\pm}(n) = {} & u_9^{\pm}(n) - \frac{dot(u_9^{\pm}(n), v_3^{\pm}(n))}{||v_3^{\pm}(n)||^2} v_3^{\pm}(n) \\ & - \frac{dot(u_9^{\pm}(n), v_5^{\pm}(n))}{||v_5^{\pm}(n)||^2} v_5^{\pm}(n) \\ & - \frac{dot(u_9^{\pm}(n), v_7^{\pm}(n))}{||v_7^{\pm}(n)||^2} v_7^{\pm}(n). \end{aligned} \tag{26}$$

Despite the reduced complexity that is achieved from the proposed sequential DPD learning, the learning time is now increased compared to the case when we learn all the DPD nonlinearity orders concurrently. Two algorithm modifications are thus proposed in the next section for improving the convergence speed of the proposed DPD.

4 Improving Convergence Speed of the Proposed DPD

In the previous section, a trade-off was made between hardware complexity and convergence time. We introduce two methods to help relax the extra time that is necessary to converge sequentially. Firstly, we modify the learning rate, and secondly, we modify the starting coefficients.

The first modification involves adjusting the learning rate μ in Eq. 22 depending on the residual correlation between the observed spurious IMD at the PA output and the nonlinear basis functions representing this IMD. We allow μ to take on two values, μ_1 and μ_2 where $\mu_1 > \mu_2$. This ensures fast convergence while not sacrificing the steady state error. We also establish a threshold, γ, and a confidence metric, ν. The change to μ is decided as shown in Algorithm 1. The threshold, γ, and the confidence metric ν are chosen based on experimental results over a wide range of carrier allocation scenarios and power levels. This helps ensure that the basis functions and the spurious IMD have actually decorrelated and that we do not switch μ too soon due to fluctuations in the correlation.

Algorithm 1 Adaptive μ update procedure

```
count = 0;
μ = μ1;
while DPD Training do
    Send block;
    Receive block;
    Calculate correlation;
    if correlation < γ then
        count = count + 1;
    end
    if count ≥ ν then
        μ = μ2;
    end
end
```

The second modification involves adjusting the starting point for the DPD training. In Eq. 22, $\bar{\boldsymbol{\alpha}}(0) = \mathbf{0}$. If we were to start closer to the final coefficient, there would be less change necessary and hence the convergence time could be much faster. We propose storing the final coefficients from various transmit scenarios. Then, whenever the same transmit scenario is used again, we can retrain by starting from the previous value. The previous coefficients should be similar, but retraining allows us to overcome possible variations due to temperature, power levels, etc.

If we slightly change a TX parameter such as the gain of the PA so that we are in a new scenario, it may not be necessary to start our training from zero. Instead, as we collect DPD coefficients from a variety of scenarios, we can perform a linear interpolation to fill in the blanks. By starting the DPD training from an interpolated guess, we can reduce the training time for new scenarios.

5 Overall DPD System Flow

In this section, the overall flow of the proposed DPD processing is summarized and presented, thus putting all the bits and pieces together. In Fig. 2, we introduce the system architecture for the DPD learning. This architecture shows the lower-level algorithm for performing the DPD learning. This architecture will be used in a method shown by the higher-level flow chart in Fig. 3 which presents the overall DPD system processing including the iterative IMD learning, sequential learning for the higher nonlinearity orders, and the speed-up methods.

The system begins by applying stored coefficients if they are available. If they are not available, the system will interpolate from other previously stored values if possible or set the DPD coefficients to zero. The system searches for spurious emissions in violation of a threshold. If there is a violation, the system chooses the most extreme violation to train on. We then choose the lowest possible order to train on for that spur (third for IM3, fifth for IM5, etc.) and perform a sub-band DPD learning step after which the spurious emissions are checked to see whether they already meet the emission requirements or not. If they do not satisfy emission requirements, an additional nonlinearity order is added. In all the learning phases, the DPD learning rate μ is varied according to the residual correlation between the observed IMD emissions and the corresponding basis function(s), in order to improve the learning speed, as explained in Algorithm 1.

Once the spurious emission is below the threshold, we search for another spur that is above the limit. If there is one, we will similarly train on that spur. We then begin the search again realizing that it is possible that a previously trained spur may no longer meet the requirements due to the mutual effects of one DPD application on the other. In the case that the DPD can not sufficiently suppress the spurious emission below the limit, we lower the transmit power and begin again. Whenever all spurs are under the limit, the coefficients can be stored in the memory. This serves as a starting point for whenever the transmission scenarios are repeated and for interpolation of other values. In the next section, experimental results are presented using the WARPLab setup demonstrating the effectiveness of the proposed DPD solution.

6 WARPLab Results

The methods presented previously in the paper were tested using the WARPLab framework on the WARPv3 board. WARP is a software-defined radio platform that allows for rapid prototyping by interfacing with MATLAB to perform the baseband signal processing [24]. The WARP board is similar to other SDR boards like the popular USRP boards from Ettus Research/National Instruments in that they allow for rapid prototyping via software such at MATLAB. In order to study the DPD performance, a PA is needed as part of the SDR platform. The USRP does not contain an integrated PA. However, the WARP platform contains a standard

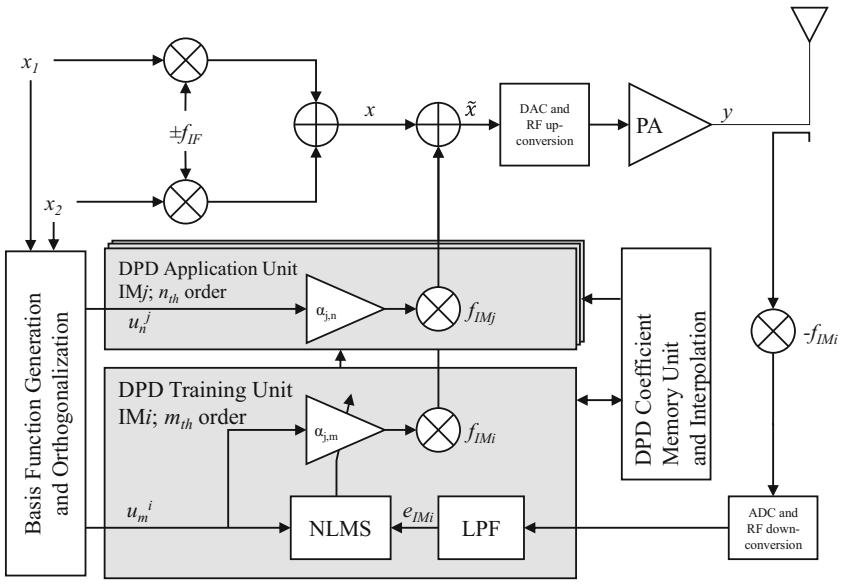

Figure 2 Block diagram of the system architecture. Here, the m^{th} nonlinear order IMi sub-band is being trained.

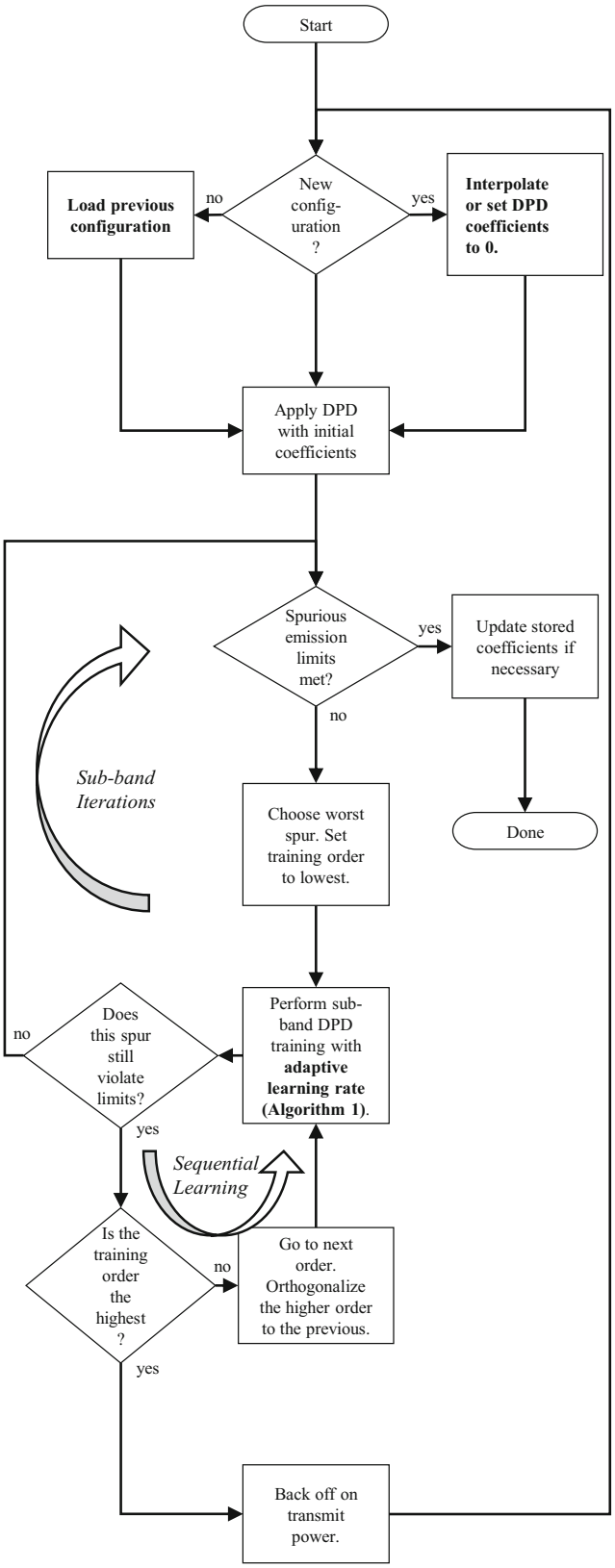

Figure 3 System flow chart of the proposed iterative sub-band DPD solution with speed-up methods. The speed-up methods are indicated in bold letters.

on-board PA which makes it ideal for algorithm verification. A photo of the experimental setup is shown in Fig. 4. For these experiments, the DPD processing is done on the host CPU, but the broadcasting is done on the WARP radio hardware which includes the Maxim MAX2829 transceiver and the Anadigics AWL6951 PA.

6.1 IM3± Iterations

We began by testing the iterative method presented in Section 2. An LTE uplink signal was generated in MATLAB with two non-contiguous carriers. One carrier was 3 MHz, and the other was 1.4 MHz. Both carriers had 64 QAM subcarrier modulation. The frequency domain results at each iteration are shown in Fig. 5. The IM3+ spur was trained first using seventh-order DPD processing, and suppression was achieved as evident in the red curve. However, the IM3- spur magnitude was increased slightly which is consistent with Eq. 7. We then trained the IM3- spur (yellow curve). Again, there was a negative effect on the opposite spur, so we retrained the IM3+ spur (purple curve). At this point, we were satisfied with the performance and quit training.

6.2 Sequential Learning

As presented in Section 3, we then tested the sequential learning concept in WARPLab where we started with low-order nonlinearities and added higher orders as needed. In Fig. 6, we show an example for comparison using the previously developed concurrent training method. We then switched to using the new sequential method as seen in Fig. 7. For these two experiments, the same LTE uplink signal and

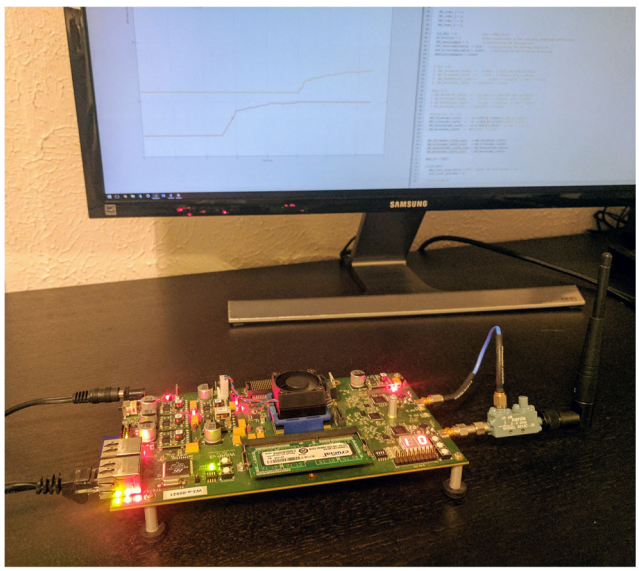

Figure 4 The WARPv3 board interfaces with MATLAB via an Ethernet cable connected to a PC. The TX port is directly connected to the RX port via a 30 dB directional coupler for the feedback loop during training.

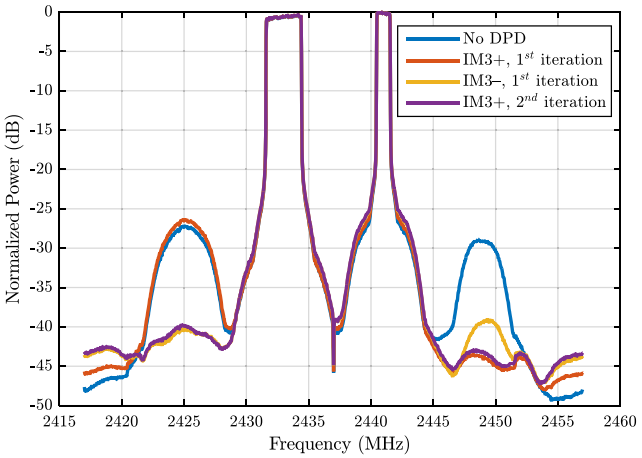

Figure 5 Normalized spectral result when using the iterative method to suppress both the IM3+ and the IM3- spurs.

setup were used. We see that all the coefficients converged to approximately the same value. In Fig. 8, we show the results in the frequency domain on the IM3+ spur. From these figures, it is evident that the final result is equivalent and the only difference is the amount of time it takes to train.

6.3 Speed-up Methods

The convergence time for sequential training is longer than training in parallel as discussed earlier and shown in Figs. 6 and 7. To overcome this, we tested the previously presented methods for speeding up the convergence time.

We tested the adaptive μ concept presented by Algorithm 1. In Fig. 9, we show the correlation between the error block and the LMS reference block as the algorithm converges. As the DPD coefficient convergences (shown in blue), the correlation decreases (shown in orange). When it is below

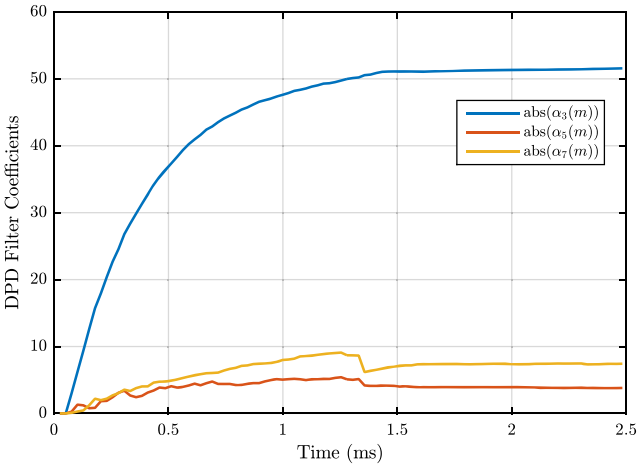

Figure 6 Example DPD coefficient convergence when concurrent training is used. By training multiple orders concurrently, convergence occurs more rapidly at the price of additional hardware complexity when compared to sequential learning.

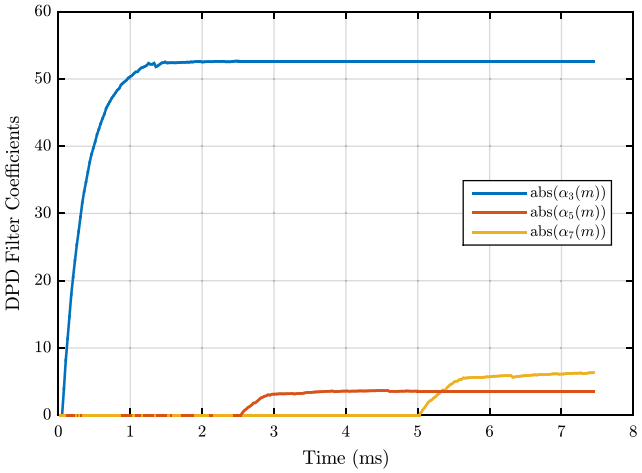

Figure 7 WARPLab testing of sequential learning of DPD coefficients. By training multiple orders sequentially, convergence occurs more slowly with the benefit of less hardware complexity when compared to concurrent learning.

the threshold (γ) of 0.05 (shown in red) more than 5 times (the confidence metric, ν), the learning rate changes from $\mu = 4$ to $\mu = 0.7$. This change of μ is denoted by the dashed line. The values were determined experimentally to what worked well for a variety of scenarios as determined by the authors.

We then tested the concept of starting the DPD coefficient at a value based on the interpolation of other trained values. When using WARPLab, there is an RF gain parameter that sets the gain for the PA. This value is an integer between zero and sixty-three with approximately half a dB of gain per integer increase of this parameter. We started with an RF gain parameter of 45 where we trained from a starting point of zero. Then, we increased the RF gain to 55 where we again trained from 0. At each, the coefficients converged smoothly with sufficient suppression.

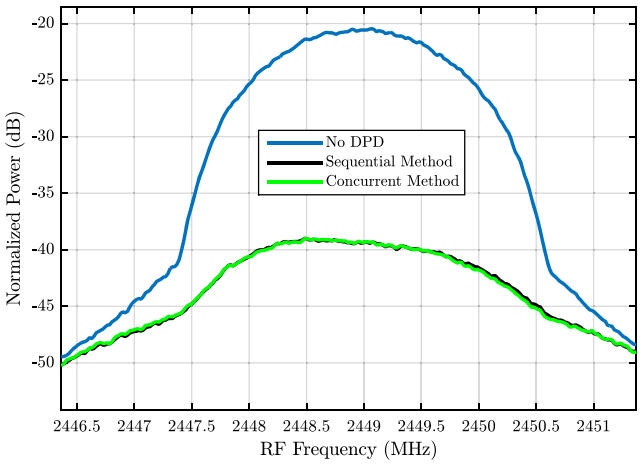

Figure 8 PSD result when using the concurrent and sequentially trained coefficients to suppress the IM3+ spur. This shows nearly identical performance between the methods.

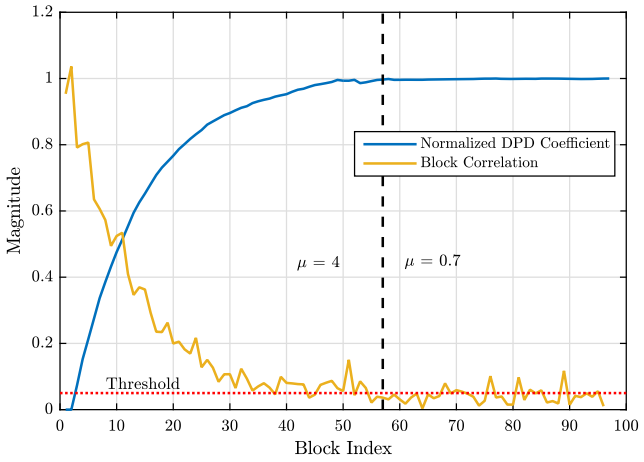

Figure 9 Correlation vs. block index during DPD training. As training progresses the correlation decreases. Once it is below the threshold for a total number of times greater than the confidence metric, we change to the lower learning rate.

We then choose to work at an RF gain of 50. We linearly interpolated from the two values previously stored. We then started training from this point. The training is shown in Fig. 10. Based off the sequential, LMS training, a small update to the interpolation guess is made.

As we continue to transmit under various conditions, the interpolations become more accurate. Eventually, a complete table of DPD coefficients is formed. Then whenever we need to broadcast, we can simply load the previous coefficients and quickly update them to account for small fluctuations if needed.

6.4 Full System Verification

We then put everything together in WARPLab to follow the process shown in Fig. 3 where multiple spurs need to be

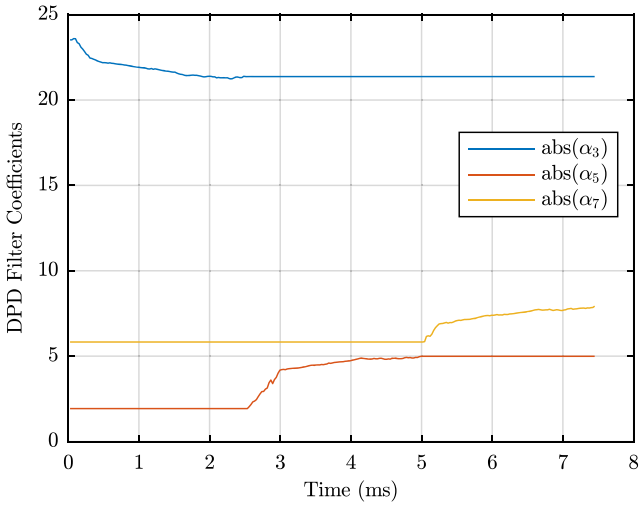

Figure 10 Convergence of the DPD coefficients after interpolating from previously learned coefficients.

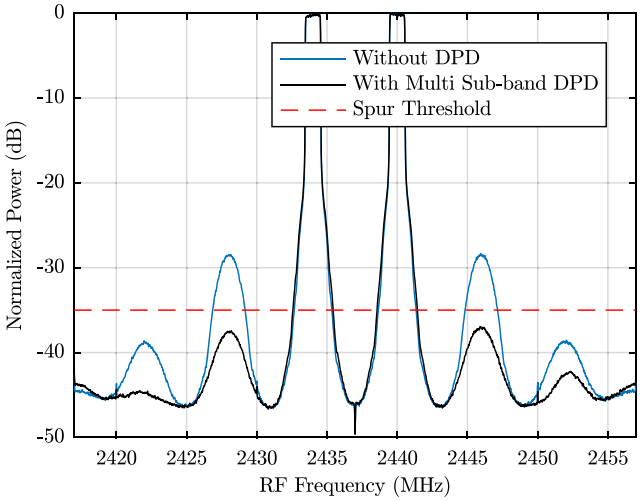

Figure 11 Normalized spectral result when using the iterative method to make sure both IM3 and both IM5 spurious emissions are below the threshold.

under a threshold. The previously discussed speed-up methods are applied in the training process. Two LTE carriers are broadcast. The two carriers are set to be 1.4 MHz LTE uplink signals spaced 6 MHz apart. This allowed the IM5 spurs to be observable in the WARP board's 40 MHz RF Bandwidth. For this experiment, we set a threshold that the spurs must be 35 dB below the main carriers. The results are plotted in Fig. 11.

We assume this to be a new configuration where we start with no know coefficients; every coefficient gets initialized to zero. The non-contiguous signal is broadcast over the WARP board, and the spectrum for this is shown as the blue curve in Fig. 11. We identify the IM3+ spur as the most severe and train on it. There is some suppression, but it does not completely meet the threshold. We train another order on the IM3+ spur and then continue the process until the

Table 1 Results of the intermediate training steps in the multi sub-band DPD from Fig. 11.

Training Step			Result (dB)			
Step	Spur	Order	IM5-	IM3-	IM3+	IM5+
0	–	–	−38.7	−28.0	−27.9	−38.8
1	IM3+	3	−37.3	−27.4	−34.4	−36.7
2	IM3+	5	−37.2	−27.4	−36.9	−36.4
3	IM3-	3	−35.9	−33.9	−35.5	−34.9
4	IM3-	5	−35.0	−37.0	−35.8	−34.5
5	IM5+	5	−34.5	−33.15	−34.5	−43.0
6	IM3-	5	−33.6	−37.1	−34.3	−44.4
7	IM5-	5	−42.9	−32.0	−33.5	−44.0
8	IM3-	5	−45.1	−37.6	−33.2	−44.0
9	IM3+	3	−43.2	−32.3	−36.8	−42.6
10	IM3-	5	−44.6	−37.5	−37.0	−42.5

final result shown in black is achieved. During the process, the mutual effect of one DPD training negatively impacts the other spurs and causes additional steps in the multi sub-band DPD. All of the intermediate results are shown Table 1.

7 Conclusion

In this paper, an iterative, multi sub-band DPD learning algorithm has been presented that can suppress the IM3 and IM5 spurious emissions. A sequential learning procedure where higher nonlinearity orders were added one at a time was also presented in order to reduce the complexity and add flexibility to the DPD solution. Additionally, the convergence speed of the proposed DPD has been improved by two methods, while not sacrificing the DPD performance. The first used a variable learning rate which switches from high speed to lower speed once the loop becomes close to convergence. The second method starts the DPD learning from previously learned points and uses interpolation of past scenarios to reduce convergence time. A WARPLab implementation of the proposed DPD solution has been demonstrated showing excellent performance with up to 20 dB suppression in the undesired spurious emissions.

Acknowledgments This work was supported by the Finnish Funding Agency for Technology and Innovation (Tekes) under the project "Future Small-Cell Networks using Reconfigurable Antennas (FUNERA)." This work was also supported in part by the US National Science Foundation under grants ECCS-1408370, ECCS-1232274, CNS-1265332, and CNS-1717218 in the WiFiUS program. The work was also funded by the Academy of Finland under the projects 288670 "Massive MIMO: Advanced Antennas, Systems and Signal Processing at mm-Waves," 284694 "Fundamentals of Ultra Dense 5G Networks with Application to Machine Type Communication," and 301820 "Competitive Funding to Strengthen University Research Proles," and by the Linz Center of Mechatronics (LCM) in the framework of the Austrian COMET-K2 program.

References

1. White paper: Cisco VNI Forecast and Methodology, 2015-2020. https://www.cisco.com/c/en/us/solutions/collateral/service-provider/visual-networking-index-vni/complete-white-paper-c11-481360.html (2016).
2. Staple, G., & Werbach, K. (2004). The end of spectrum scarcity: spectrum allocation and utilization. *IEEE Spectrum*, *41*, 48–52.
3. Tarazi, I. (2017). Solving The Spectrum Challenge. http://www.federatedwireless.com/solving-the-spectrum-challenge/ Federated Wireless.
4. Wannstrom, J. (2013). Carrier Aggregation Explained. http://www.3gpp.org/technologies/keywords-acronyms/101-carrier-aggregation-explained. 3GPP.
5. Khan, Z., Ahmadi, H., Hossain, E., Coupechoux, M., Dasilva, L.A., Lehtomäki, J.J. (2014). Carrier aggregation/channel bonding in next generation cellular networks: methods and challenges, *IEEE Network*, *28*, 34–40.
6. Ghannouchi, F.M., & Hammi, O. (2009). Behavioral modeling and predistortion. *IEEE Microwave Magazine*, *10*, 52–64.
7. Park, C.S., Sundström, L., Wallén, A., Khayrallah, A. (2013). Carrier aggregation for lte-advanced: design challenges of terminals. *IEEE Communications Magazine*, *51*, 76–84.
8. Abdelaziz, M., Fu, Z., Anttila, L., Wyglinski, A.M.,Valkama, M. (2016). Digital predistortion for mitigating spurious emissions in spectrally agile radios. *IEEE Communications Magazine*, *54*, 60–69.
9. Nokia, R4-121205 Way forward for non-contiguous intraband transmitter aspects. Available at: http://www.3gpp.org/, tech. rep., 3GPP (2013).
10. Nokia, R4-124353, Non-contiguous intraband unwanted emission. Available at: http://www.3gpp.org/, tech. rep., 3GPP (2013).
11. Lähteensuo, T. (2013). *Linearity requirements in LTE advanced mobile transmitter.* Master's thesis. Tampere: Tampere University of Technology.
12. Braithwaite, R.N. (2013). A combined approach to digital predistortion and crest factor reduction for the linearization of an RF power amplifier. *IEEE Transactions on Microwave Theory and Techniques*, *61*, 291–302.
13. Roblin, P. Myoung, S.K., Chaillot, D., Kim, Y.G., Fathimulla, A., Strahler, J., Bibyk, S. (2008). Frequency-selective predistortion linearization of RF power amplifiers. *IEEE Transactions on Microwave Theory and Techniques*, *56*, 65–76.
14. Kim, J., Roblin, P., Chaillot, D., Xie, Z. (2013). A generalized architecture for the frequency-selective digital predistortion linearization technique. *IEEE Transactions on Microwave Theory and Techniques*, *61*, 596–605.
15. Bassam, S., Helaoui, M., Ghannouchi, F. (2012). Channel-selective multi-cell digital predistorter for multi-carrier transmitters. *IEEE Transactions on Microwave Theory and Techniques*, *60*, 2344–2352.
16. Abdelaziz, M., Anttila, L., Mohammadi, A., Ghannouchi, F., Valkama, M. (2014). Reduced-complexity power amplifier linearization for carrier aggregation mobile transceivers. In *IEEE international conference on acoustics, speech, and signal processing*.
17. Katz, A., Wood, J., Chokola, D. (2016). The evolution of pa linearization: from classic feedforward and feedback through analog and digital predistortion. *IEEE Microwave Magazine*, *17*, 32–40.
18. Bassam, S., Ghannouchi, F., Helaoui, M. (2011). 2-D digital predistortion (2-D-DPD) architecture for concurrent dual-band transmitters. *IEEE Transactions on Microwave Theory and Techniques*, *59*, 2547–2553.
19. Dano, M. ATT: We are deploying 3-channel carrier aggregation on LTE network. http://www.fiercewireless.com/wireless/at-t-we-are-deploying-3-channel-carrier-aggregation-lte-network.
20. Qualcomm, Snapdragon 835 processor specs. https://www.qualcomm.com/products/snapdragon/ processors/835.
21. Abdelaziz, M., Tarver, C., Li, K., Anttila, L., Valkama, M., Cavallaro, J. (2015). Sub-band digital predistortion for noncontiguous transmissions: algorithm development and real-time prototype implementation. In *49th asilomar conference signals, systems, and computers.* Pacific, Grove, CA, USA.
22. Tarver, C., Abdelaziz, M., Anttila, L.. Valkama, M., Cavallaro, J.R. (2016). Low-complexity, sub-band dpd with sequential learning: Novel algorithms and warplab implementation. In *2016 IEEE international workshop on signal processing systems (SiPS)* (pp. 303–308).
23. Abdelaziz, M., Anttila, L., Tarver, C., Li, K., Cavallaro, J.R., Valkama, M. (2016). Low-complexity subband digital predistortion for spurious emission suppression in noncontiguous spectrum access. *IEEE Transactions on Microwave Theory and Techniques*, *64*, 3501–3517.
24. WARP Project. http://warpproject.org.

Chance Tarver received the B.S. degree in electrical engineering from Louisiana Tech University, Ruston, LA, in 2014, and the M.S. degree in electrical and computer engineering in 2016 from Rice University, Houston, TX. He is currently a Ph.D. student in the Department of Electrical and Computer Engineering at Rice University. His research interests include efficient architectures for wireless communications signal processing, spectrum sharing, and software-defined radios.

Mahmoud Abdelaziz received his D.Sc. (with honors) degree in Electronics and Communications Engineering from Tampere University of Technology, Finland, in 2017. He received his B.Sc. (with honors) and M.Sc. degrees in Electronics and Communications Engineering from Cairo University, Egypt, in 2006 and 2011, respectively. He currently works as a Postdoctoral researcher at Tampere University of Technology, Finland. From 2007 to 2012 he has been working as a communication systems, signal processing, and embedded systems engineer at Newport Media Inc. (Egypt design center), Etisalat Egypt, and Axxcelera Egypt Broadband Wireless. His research interests include statistical and adaptive signal processing in flexible radio transceivers, in particular, behavioral modeling and digital pre-distortion of power amplifiers in single and multiple antenna transmitters.

Lauri Anttila (S'06, M'11) received the M.Sc. degree and the D.Sc. (Tech) degree (with honors) in electrical engineering from Tampere University of Technology (TUT), Tampere, Finland, in 2004 and 2011. Since 2016, he has been a senior research fellow at the Laboratory of Electronics and Communications Engineering at TUT. In 2016-2017, he was a visiting research fellow at the Department of Electronics and Nanoengineering, Aalto University, Finland. His research interests are in signal processing for wireless communications, hardware constrained communications, and radio implementation challenges in 5G cellular radio, full-duplex radio, and large-scale antenna systems. He has co-authored over 80 peer reviewed articles in these areas, as well as three book chapters.

Mikko Valkama (S'00'M'01' SM'15) was born in Pirkkala, Finland, on November 27, 1975. He received the M.Sc. and Ph.D. Degrees (both with honors) in electrical engineering (EE) from Tampere University of Technology (TUT), Finland, in 2000 and 2001, respectively. In 2002, he received the Best Ph.D. Thesis -award by the Finnish Academy of Science and Letters for his dissertation entitled "Advanced I/Q signal processing for wideband receivers: Models and algorithms". In 2003, he was working as a visiting post-doc research fellow with the Communications Systems and Signal Processing Institute at SDSU, San Diego, CA. Currently, he is a Full Professor and Laboratory Head at the Laboratory of Electronics and Communications Engineering at TUT, Finland. His general research interests include radio communications, communications signal processing, estimation and detection techniques, signal processing algorithms for flexible radios, cognitive radio, full-duplex radio, radio localization, and 5G mobile cellular radio networks.

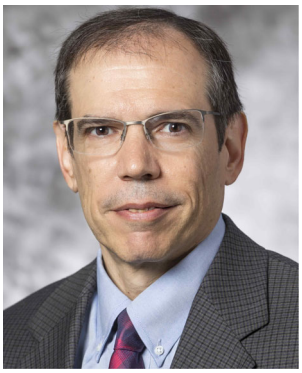

Joseph R. Cavallaro received the B.S. degree from the University of Pennsylvania, Philadelphia, Pa, in 1981, the M.S. degree from Princeton University, Princeton, NJ, in 1982, and the Ph.D. degree from Cornell University, Ithaca, NY, in 1988, all in electrical engineering. From 1981 to 1983, he was with AT&T Bell Laboratories, Holmdel, NJ. In 1988, he joined the faculty of Rice University, Houston, TX, where he is currently a Professor of electrical and computer engineering. His research interests include computer arithmetic, and DSP, GPU, FPGA, and VLSI architectures for applications in wireless communications. During the 1996–1997 academic year, he served at the National Science Foundation as Director of the Prototyping Tools and Methodology Program. He was a Nokia Foundation Fellow and a Visiting Professor at the University of Oulu, Finland in 2005 and continues his affiliation there as an Adjunct Professor. He is currently the Director of the Center for Multimedia Communication at Rice University. He is an advisory board member of the IEEE SPS TC on Design and Implementation of Signal Processing Systems and the Chair-Elect of the IEEE CAS TC on Circuits and Systems for Communications. He is currently an Associate Editor of the IEEE Transactions on Signal Processing, the IEEE Signal Processing Letters, and the Journal of Signal Processing Systems. He was Co-chair of the 2004 Signal Processing for Communications Symposium at the IEEE Global Communications Conference and General/Program Co-chair of the 2003, 2004, and 2011 IEEE International Conference on Application-Specific Systems, Architectures and Processors (ASAP), General/Program Co-chair for the 2012, 2014 ACM/IEEE GLSVLSI, Finance Chair for the 2013 IEEE GlobalSIP conference, TPC Co-Chair of the 2016 IEEE SiPS workshop, and TPC Chair of the 2017 IEEE Asilomar Conference on Signals, Systems, and Computers. He served on the IEEE CAS Society Board of Governors during 2014 and is a Fellow of the IEEE.